

Phase Change Materials for Nonvolatile, Solid-State Reflective Displays: From New Structural Design Rules to Enhanced Color-Changing Performance

Shuaipeng Tao, Qian Li, Jiafu Wang, Xiaoyi Wang, Jize Cai, Shibo Li, Wei Xu, Kan Zhang, and Chaoquan Hu*

With the arrival of omnimedia era, there has been an increasing demand for energy-saving, colorful, and portable displays. Traditional display technologies, such as electrophoresis and electronic ink display suffer from low color switching speed and poor color richness. Due to their high performances, phase change materials (PCMs)-based nonvolatile, solid-state reflective display coatings have become the most promising materials for new portable display technology. Existing researches mainly focus on improving the color-changing performance of coatings by optimizing film structural parameters, but ignore improving the performance by designing new PCMs. Here, this study reveals the color-changing mechanisms of display coatings through a combination of experiments, first-principles calculations, spectral fitting, and optical simulation. It is found that reducing the vacancy concentrations of PCMs can increase the color-changing performance of coatings owing to the increase in p-p coupling strength. Based on previous reports and the new insights into p-p coupling strength, this study proposes three structural design principles of ideal PCMs (low ionicity, a limited degree of hybridization, and high p-p coupling strength) and predicts new PCM candidates for display applications. This study opens a broad avenue for developing nonvolatile display technologies and material selection.

can rapidly convert from amorphous to crystalline states under appropriate electrical/optical/thermal excitation.^[1–8] During transformation from amorphous to crystalline states, the chemical bonds and degree of order of PCMs change significantly.^[9–13] As a result, their electrical and optical properties also change drastically.^[12,14–16] Because of the variability of their electrical properties (mainly resistance), PCMs have been widely used in nonvolatile electric fields, such as high-density memories.^[17–23] Because of the variability of their optical properties (mainly optical constants,^[9,24,25] reflectivity,^[26,27] transmission,^[25,28,29] absorption,^[30,31] and emissivity^[32]), PCMs been widely applied in nonvolatile photonic applications, such as all-photonic memories,^[26,33,34] active absorbers,^[35] filters,^[25] lenses,^[34,36] sensors,^[36] displays, etc.^[26,27,37–39] Among the above optical applications, the PCM-based solid-state reflective display^[27] is a revolutionary display technology. It has many advantages, such as high resolution, rich colors, and fast color switching over tra-

ditional technologies, such as electrophoresis and electronic ink display. The PCM-based solid-state reflective display has become the most promising portable display technology.


Current research on PCM-based nonvolatile coatings for displays mainly focuses on designing multilayer film structures and improving their color-changing properties. Specifically, the related research can be roughly summarized into three aspects. First, Hosseini et al.^[26,27,40] pioneered the new concept of PCM-based “non-volatile displays” in 2014, and then designed and developed Ge₂Sb₂Te₅- and Ag₃In₄Sb₇Te₁₇-based four-layer display coatings with a metal/transparent dielectric/PCM/transparent dielectric structure. These coatings have high resolution, color tunability, and broad color gamut,^[10] and thus can be applied to various opaque/transparent and rigid/soft substrates. Second, Cheng et al.,^[41,42] and Liu,^[43] et al. systematically studied the effect of the thicknesses of transparent dielectric layer and Ge₂Sb₂Te₅ layer on the color rendering performance of coatings. They extended the color gamut of the coatings by optimizing the thickness of each film. Besides, they developed a Ge₂Sb₂Te₅-based three-layer film system, which could reduce

1. Introduction

Chalcogenide phase change materials (PCMs) refer to alloy materials that include at least one chalcogenide element and

S. Tao, Q. Li, J. Wang, J. Cai, S. Li, W. Xu, Prof. K. Zhang, Prof. C. Hu
 State Key Laboratory of Superhard Materials
 Key Laboratory of Automobile Materials of Ministry of Education
 School of Materials Science and Engineering
 Jilin University
 Changchun 130012, China
 E-mail: cqhu@jlu.edu.cn

Prof. X. Wang
 Key Laboratory of Optical System Advanced Manufacturing Technology
 Changchun Institute of Optics
 Fine Mechanics and Physics
 Chinese Academy of Sciences
 Changchun 130033, China

 The ORCID identification number(s) for the author(s) of this article can be found under <https://doi.org/10.1002/adom.202000062>.

DOI: 10.1002/adom.202000062

both manufacturing costs and energy loss. Third, Yoo et al.,^[44] Ji et al.,^[45] and Jafari et al.^[46] replaced the single $\text{Ge}_2\text{Sb}_2\text{Te}_5$ layer with double PCM layers including thin $\text{Ge}_2\text{Sb}_2\text{Te}_5$ /thick $\text{Ge}_2\text{Sb}_2\text{Te}_5$, SbTe/GeTe , and thin GeTe /thick GeTe , respectively. Because of the difference in phase transition temperature between the two PCM layers, the double-layer PCM structures were found to have increased color richness and color gamut during annealing. The proposed new structures and methods have greatly improved the color-changing performances of PCM coatings and greatly promoted the development of PCM-based nonvolatile displays.

According to the Fabry–Perot interference,^[44,47] the color-changing performance of PCM-based multilayer coatings originates from the dramatic change of the visible reflectance of PCM caused by phase change. Two main factors can affect the reflectance of multilayer display coatings. The first one is film structure. Film structure refers to the composition of multilayer film and the thickness of each component layer, wherein the composition means the number and arrangement of the component layers including dielectric, PCM, and metal mirror layers. The influence of these structural parameters on the color-changing performances of display coatings has been systematically reported in previous studies. The second factor is the choice of PCMs. Studies have shown that PCMs with high optical contrast have low ionicity and limited degree of sp^3 -hybridization. The PCMs meeting these two conditions are mainly Te-based binary or ternary materials, such as GeTe , Sb_2Te_3 , $\text{Ge}_2\text{Sb}_2\text{Te}_5$, $\text{Ge}_1\text{Sb}_2\text{Te}_4$, and so on. It is expected that for display coatings containing different PCMs, the variation of their optical constants (n and k) and reflectance spectra caused by phase change is different, and their color-changing performances will also be different. However, previous studies have mainly explored the effect of film structure on the color-changing performance of coatings. The effect of different PCM incorporation has not yet been reported, and it remains unclear how to design PCMs at the atomic level to improve the color-changing performance of display coatings. Moreover, although the phase change of PCM film leads to the color change of multilayer display coatings, the underlying mechanism is still unclear. The effect of phase change on the optical constants (n and k) of PCMs and consequently the color-changing performances of multilayer display coatings is still not well understood. These problems have greatly limited the development of nonvolatile coatings for display technology and brought open challenges to material researchers.

In this work, we revealed the color-changing mechanism of PCM-based multilayer coatings and proposed the structural design principles of PCMs for high color-changing performance through a combination of experiments, first-principles calculations, spectral fitting, and optical simulation. By studying the intrinsic relationship among phase transition, electronic structure, optical constant, and color changing of PCMs, we revealed the microscopic mechanism of the color-changing behavior of PCMs. By studying the relationship between the phase change of PCMs (GeTe , $\text{Ge}_8\text{Sb}_2\text{Te}_{11}$, $\text{Ge}_3\text{Sb}_2\text{Te}_6$, $\text{Ge}_2\text{Sb}_2\text{Te}_5$, $\text{Ge}_1\text{Sb}_2\text{Te}_4$) with different vacancy concentrations and the optical properties of display coating with a structure of ITO/PCM/ITO/Ag (IPIA), we found that a reduction in vacancy concentration can significantly increase the color-changing performance of

display coatings. This can be attributed to the high p–p coupling strength of PCMs with low vacancy concentration. Based on previous reports^[48] and our new insights into p–p coupling strength, we proposed three structural design principles of PCMs for high color-changing performance and predicted a series of candidate materials worthy of further study.

2. Results and Discussion

2.1. The Structure and Optical Constants of $\text{Ge}_2\text{Sb}_2\text{Te}_5$ and GeTe Films

Figure 1a–d shows high-resolution transmission electron microscopy (HRTEM) and grazing-incidence X-ray diffraction (GIXRD) patterns for $\text{Ge}_2\text{Sb}_2\text{Te}_5$ and GeTe films. For as-deposited $\text{Ge}_2\text{Sb}_2\text{Te}_5$ film, there is only one broad peak in the GIXRD pattern, indicating that the film is amorphous. When the annealing temperature (T_a) reaches 250 °C, the (111), (200), (220), and (222) peaks/rings of face centered cubic structure appear in the GIXRD and selected area electron diffraction (SAED) patterns of $\text{Ge}_2\text{Sb}_2\text{Te}_5$, and periodic lattice and (200) and (220) crystal faces are clearly displayed on the HRTEM of $\text{Ge}_2\text{Sb}_2\text{Te}_5$. These results are in good agreement with each other and prove that the film changes from amorphous phase (a- $\text{Ge}_2\text{Sb}_2\text{Te}_5$) to crystalline cubic phase (c- $\text{Ge}_2\text{Sb}_2\text{Te}_5$) at 250 °C. A similar phenomenon was observed in GeTe film. The as-deposited GeTe film is amorphous (a- GeTe), and after annealing at 250 °C, the structure changes to a crystalline rhombohedral phase (c- GeTe).

The refractive index, extinction coefficient, the real part (ϵ_1), and imaginary part (ϵ_2) of dielectric function of a- $\text{Ge}_2\text{Sb}_2\text{Te}_5$, c- $\text{Ge}_2\text{Sb}_2\text{Te}_5$, a- GeTe , and c- GeTe are shown in Figure 1e–h. When $\text{Ge}_2\text{Sb}_2\text{Te}_5$ changes from amorphous to cubic phase, the refraction index and extinction coefficient increase greatly, the ϵ_1 changes from positive to negative, and the ϵ_2 increases greatly. These results suggest that the film changes from a low absorption state to a high absorption state, in other words, from semiconductor to metal. Similar optical property evolution also appears in GeTe film. These results consistently show that the phase change leads to significant changes in the optical properties of $\text{Ge}_2\text{Sb}_2\text{Te}_5$ and GeTe films.

2.2. The Color-Changing Performance of $\text{Ge}_2\text{Sb}_2\text{Te}_5$ - and GeTe -Based IPIA Display Coatings

An IPIA four-layer coating structure was designed and prepared on a single-crystal silicon substrate to investigate the color-changing performances of $\text{Ge}_2\text{Sb}_2\text{Te}_5$ - and GeTe -based display coatings (Figure 2a). The first layer deposited on silicon is Ag with a thickness of 100 nm and it acts as a mirror. The second layer is the ITO layer with a thickness from 70 to 290 nm and it is designed to adjust optical path difference. The third layer is the PCM layer ($\text{Ge}_2\text{Sb}_2\text{Te}_5$ or GeTe) with a thickness of 5 nm and it is designed to change the color of the coating. The fourth layer is another ITO layer with a thickness of 10 nm and it is designed to protect the PCM layer from oxidation.

The effect of the thickness of the second ITO layer (d) on the color of IPIA coating was investigated, and the simulated

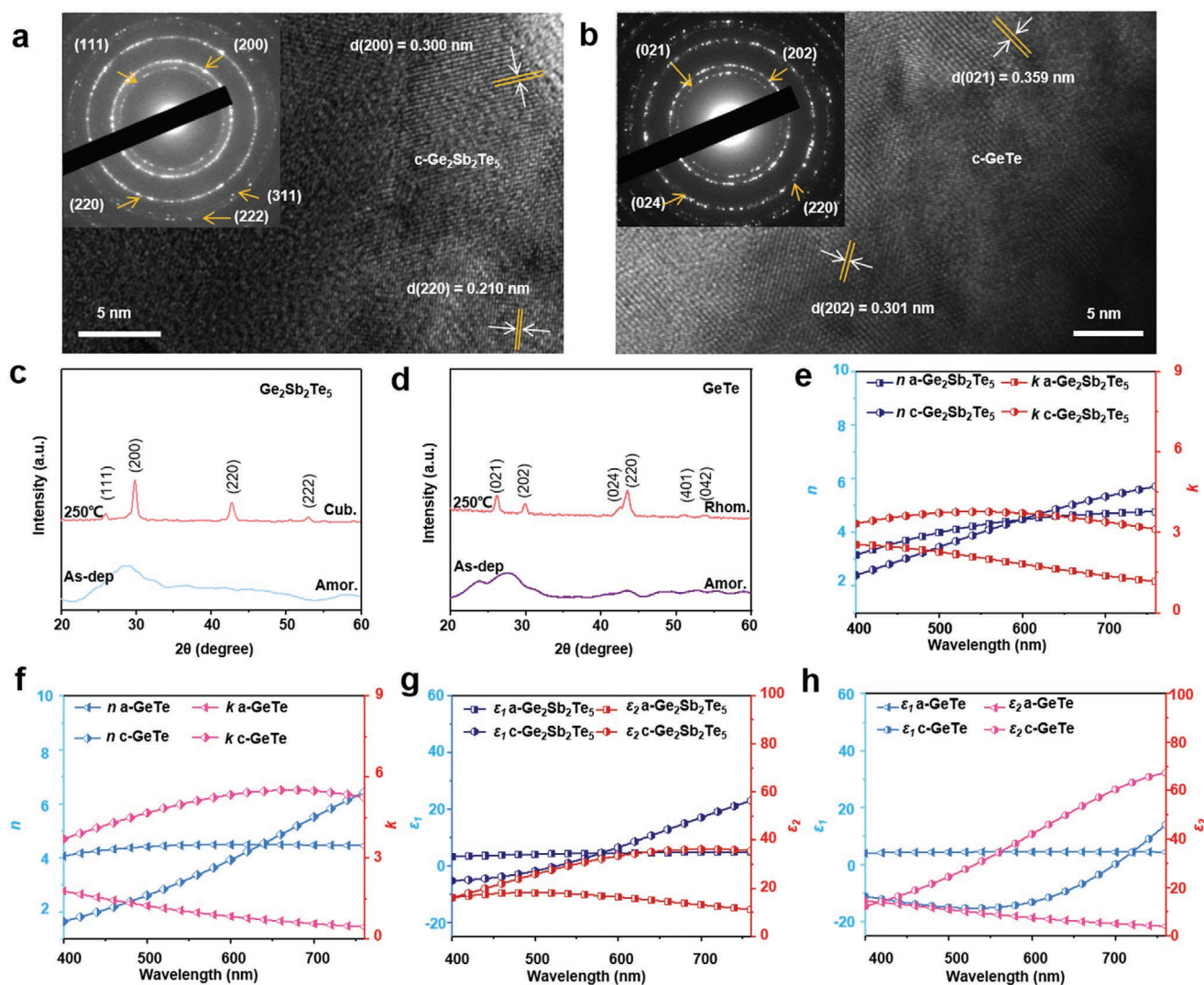


Figure 1. HRTEM lattice images of a) $\text{c-Ge}_2\text{Sb}_2\text{Te}_5$ and b) c-GeTe , inset is the SAED of the same sample; GIXRD spectra of c) $\text{Ge}_2\text{Sb}_2\text{Te}_5$ and d) GeTe in different phases; refractive index n and extinction coefficient k of e) $\text{Ge}_2\text{Sb}_2\text{Te}_5$ and f) GeTe in different phases; ϵ_1 and ϵ_2 for g) $\text{Ge}_2\text{Sb}_2\text{Te}_5$ and h) GeTe .

reflectance spectra and colors are shown in Figure 2b,c. When $d = 170, 220$, and 240 nm , the amorphous $\text{IPIA}_{\text{Ge}_2\text{Sb}_2\text{Te}_5}$ coatings are purple, blue, and light green, respectively. These three IPIA coatings were considered as three typical structures in this study. In order to verify the simulation results, we prepared these three structures. The experimental reflectance spectra and colors of the three coatings are shown in Figure 2b,c. The positions and intensities of peaks in the experimental reflectance spectra and the experimentally observed colors are in good agreement with the simulation results. This proves the reliability of simulation results. Therefore, in the following discussion, we mainly rely on simulation to investigate the difference in color-changing performance between $\text{Ge}_2\text{Sb}_2\text{Te}_5$ - and GeTe -based IPIA coatings.

The reflectance spectra of $\text{IPIA}_{\text{Ge}_2\text{Sb}_2\text{Te}_5}$ and $\text{IPIA}_{\text{GeTe}}$ coatings (Figure 2b) were analyzed. With the phase change from amorphous to crystalline phase, the reflectivity peaks of $\text{IPIA}_{\text{Ge}_2\text{Sb}_2\text{Te}_5}$ and $\text{IPIA}_{\text{GeTe}}$ coatings are all blueshifted, and the reflectivity peaks of the latter are shifted to even shorter wavelength. As

shown in Figure 2c, the color change of $\text{IPIA}_{\text{GeTe}}$ coating is more significant than that of $\text{IPIA}_{\text{Ge}_2\text{Sb}_2\text{Te}_5}$ coating. For example, the color of IPIA coating ($d = 220 \text{ nm}$) changes from blue to dark blue after phase change, while the color of GeTe changes from cyan to dark purple. These results show that $\text{IPIA}_{\text{GeTe}}$ coating has better color-changing performance than $\text{IPIA}_{\text{Ge}_2\text{Sb}_2\text{Te}_5}$ coating.

To quantify the color-changing performance of $\text{IPIA}_{\text{Ge}_2\text{Sb}_2\text{Te}_5}$ and $\text{IPIA}_{\text{GeTe}}$, we calculated their reflectivity change values ΔR after phase change ($\Delta R = R_c - R_a$), where R_a and R_c are the reflectivity of IPIA when the PCM is in amorphous and crystalline states, respectively. In Figure 3a, when $d = 170, 220$, and 240 nm , all the ΔR values of GeTe are higher than those of $\text{Ge}_2\text{Sb}_2\text{Te}_5$, and the integrated intensity of ΔR ($S(x) = \int_{400}^{760} |\Delta R_{\text{color}}(x)| dx$) for GeTe is 124.8%, 125.9%, and 141.8% higher than those of $\text{Ge}_2\text{Sb}_2\text{Te}_5$, respectively (Figure 3b). This indicates that the reflectance spectra of GeTe coating changes more significantly than those of $\text{Ge}_2\text{Sb}_2\text{Te}_5$ after phase change. To be more intuitively, the colors corresponding to the reflectance spectra are labeled in the chromaticity diagram (Figure 3c). It can be seen

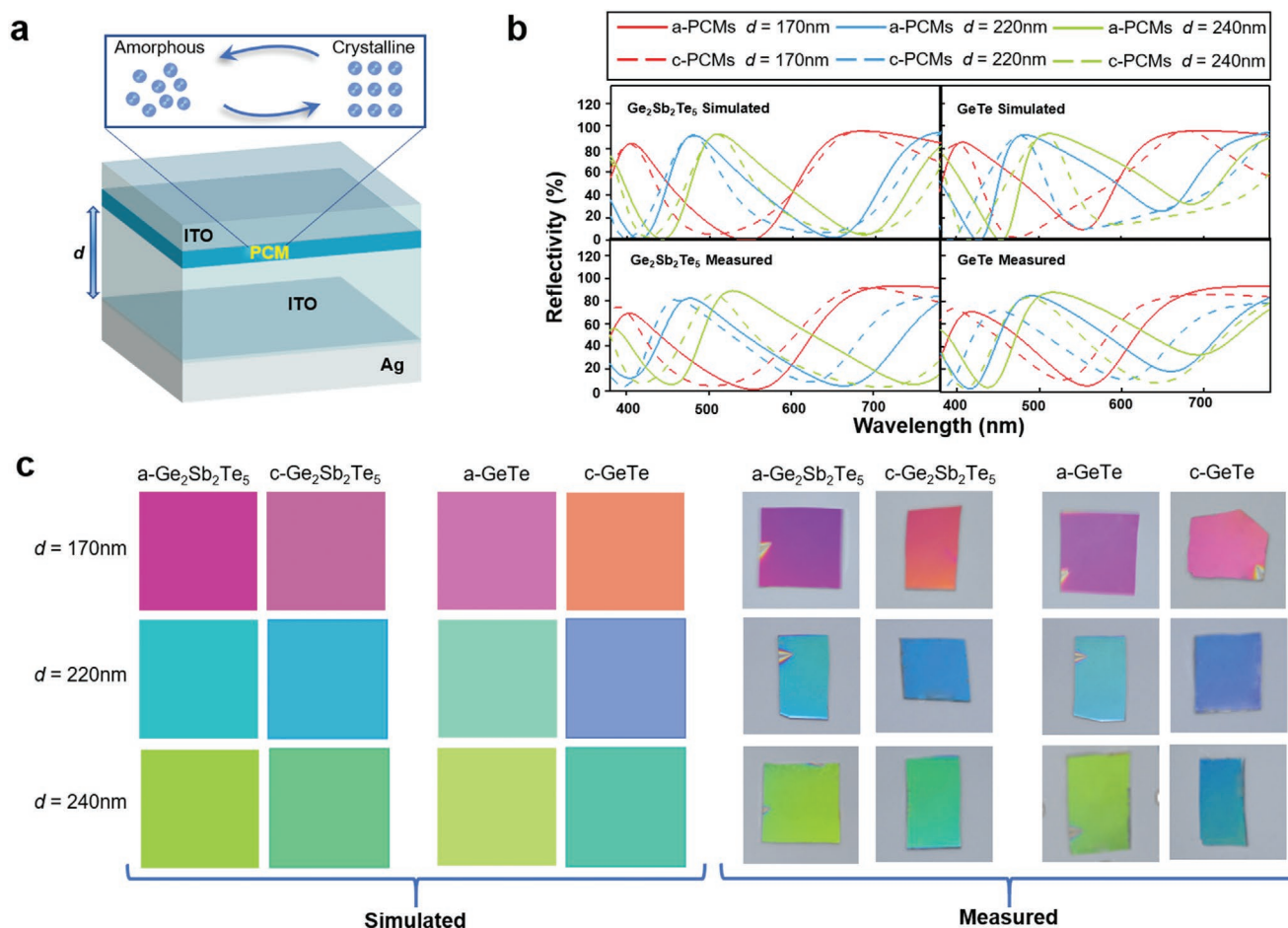


Figure 2. a) Schematic illustration of the structure of ITO/PCM/ITO/Ag coating. b) Reflectance spectra of simulated (upper left) and measured (bottom left) Ge₂Sb₂Te₅ coatings in different phase states, and reflectance spectra of simulated (upper right) and measured (bottom right) GeTe coatings in different phase states. c) The colors of simulated (left) and measured (right) Ge₂Sb₂Te₅ and GeTe coatings in different phase states.

that when $d = 170, 220$, and 240 nm, the color point of IPIA_{GeTe} coating moves farther than that of IPIA_{Ge₂Sb₂Te₅}.

To investigate the display performance of IPIA_{GeTe} and IPIA_{Ge₂Sb₂Te₅} coatings, the colors corresponding to the amorphous state were used as the background colors and the colors corresponding to the crystalline state were used to draw the LOGO of Jilin University, as shown in Figure 3d. Clearly, IPIA_{GeTe} enables more significant color differences between the background and the LOGO than IPIA_{Ge₂Sb₂Te₅} when $d = 170, 220$, or 240 nm. Figure 3e,f shows the reflectance spectra and colors of IPIA_{Ge₂Sb₂Te₅} and IPIA_{GeTe} coatings under various d (70–290 nm). It can be seen that the integrated intensity of ΔR and color-changing performance of IPIA_{GeTe} are higher than those of IPIA_{Ge₂Sb₂Te₅} for any given d .

In order to study the effect of T_a , we performed annealing of 125, 150, 175, 200, 225, and 250 °C for single layer Ge₂Sb₂Te₅ and GeTe films. The GIXRD spectra, sheet resistance, reflectance spectra and dielectric constant are shown in Figures S1–S4 (Supporting Information), respectively. When the T_a is lower than 150 °C, Ge₂Sb₂Te₅ and GeTe are amorphous with high resistance. When T_a is 175 °C, the two films are crystal with low resistance. These results mean the amorphous-crystalline phase transition points of the Ge₂Sb₂Te₅ and GeTe films are

between 150 and 175 °C, which is in good agreement with other works.^[49] As T_a increases, the reflectivity and optical constant of Ge₂Sb₂Te₅ changes slowly, while that of GeTe changes sharply, indicating that GeTe has greater optical contrast than Ge₂Sb₂Te₅. We introduce Ge₂Sb₂Te₅ and GeTe films with different T_a into the IPIA coating to obtain the corresponding colors and draw the “lotus” with these colors (Figure 4a). It can be seen that when $d = 170$ nm, Ge₂Sb₂Te₅ mainly shows two colors of purple and pink, while GeTe shows lavender and orange in addition to purple and pink. A similar situation occurs in other ITO thicknesses. When $d = 220$ nm, Ge₂Sb₂Te₅ shows two colors: blue and dark blue, while GeTe presents four colors: blue, dark blue, cyan, and dark purple. At $d = 240$ nm, Ge₂Sb₂Te₅ shows two colors: light green and green, while GeTe presents four colors: light green, green, yellow-green, and dark blue. We chose the colors of coatings at $d = 170$ nm and with different T_a (as-deposited, 150, 225, and 250 °C) to plot the “peacock” (Figure 4b). It can be seen that IPIA_{GeTe} enables clearer peacock and lotus images than IPIA_{Ge₂Sb₂Te₅}. These results are in good agreement with reflectance spectra and LOGO results, which consistently prove that GeTe-based IPIA coatings have better color richness and contrast, and thus better color-changing performance than Ge₂Sb₂Te₅-based IPIA coating.

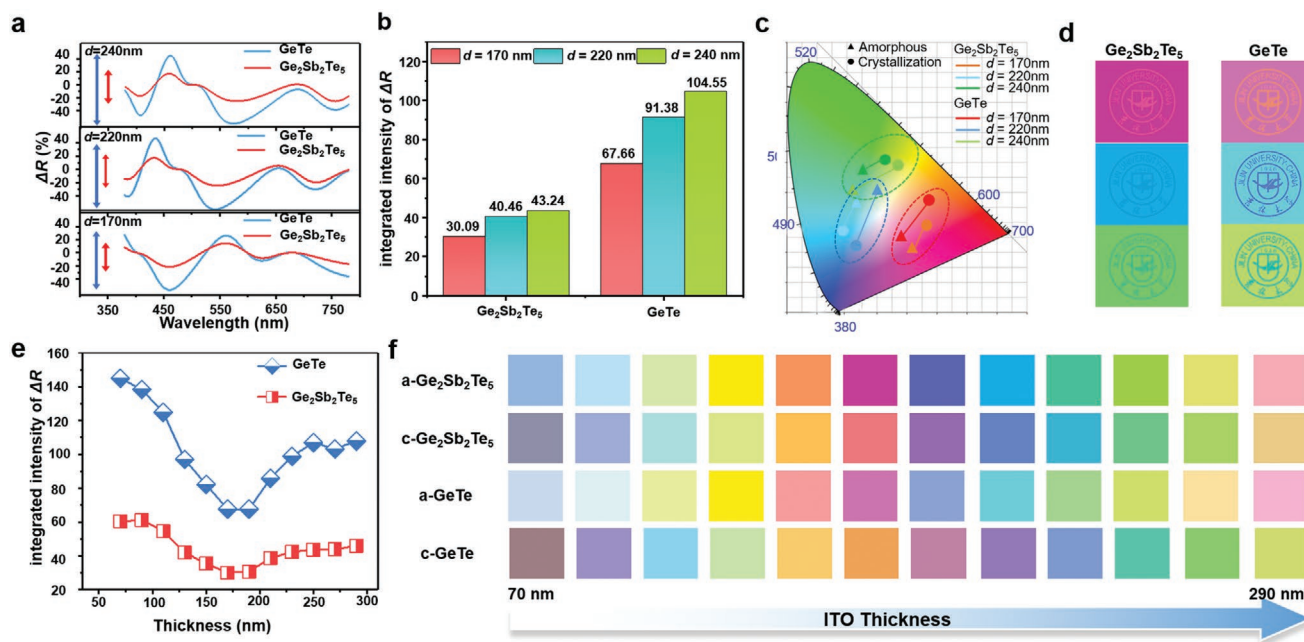


Figure 3. a) The reflectivity change ΔR , b) integrated intensity of ΔR , c) corresponding color in the chromaticity diagram and d) colorful patterns for IPIA $_{\text{Ge}_2\text{Sb}_2\text{Te}_5}$ and IPIA $_{\text{GeTe}}$ with different ITO thicknesses ($d = 170, 220$, and 240 nm). e) Integrated intensity of ΔR with $d = 70$ – 290 nm. f) The simulated colors of display coatings based on a- $\text{Ge}_2\text{Sb}_2\text{Te}_5$, c- $\text{Ge}_2\text{Sb}_2\text{Te}_5$, a- GeTe , and c- GeTe with $d = 70$ – 290 nm.

In addition to color-changing performance, cycling endurance is another important parameter for display applications. According to relevant references, the cycling endurance of GeTe is 4×10^4 – 10^5 cycles,^[50,51] which is lower than that of $\text{Ge}_2\text{Sb}_2\text{Te}_5$ (2×10^6 cycles).^[52–54] Thus, $\text{Ge}_2\text{Sb}_2\text{Te}_5$ -based displays have a better cycleability performance, while GeTe -based display should have a better color-changing performance.

2.3. Microscopic Origin of the High Color-Changing Performance of GeTe -Based IPIA Display Coatings

The color-changing performance of IPIA display coatings originates from the phase change of PCMs which causes the changes of n and k , and then the change of reflectivity. Therefore, in order to explain why IPIA $_{\text{GeTe}}$ has higher color-changing performance than

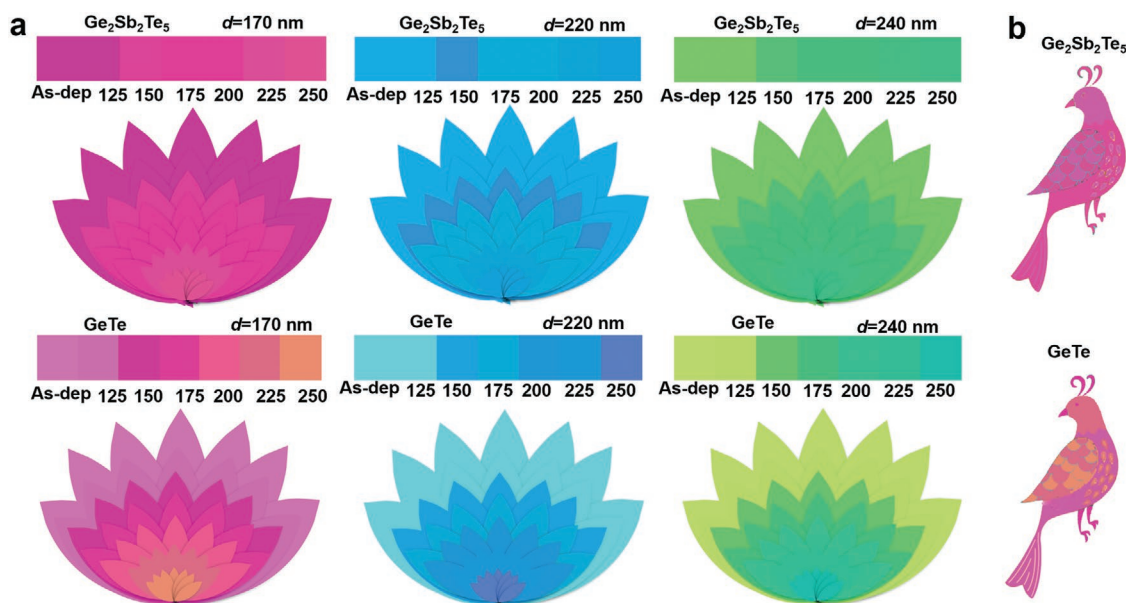


Figure 4. a) Colors of IPIA coatings with $\text{Ge}_2\text{Sb}_2\text{Te}_5$ and GeTe in different T_a and different ITO thicknesses ($d = 170, 220$, and 240 nm), and the lotus drawn with these colors. b) The peacock drawn with the colors of IPIA coatings with $d = 170$ nm.

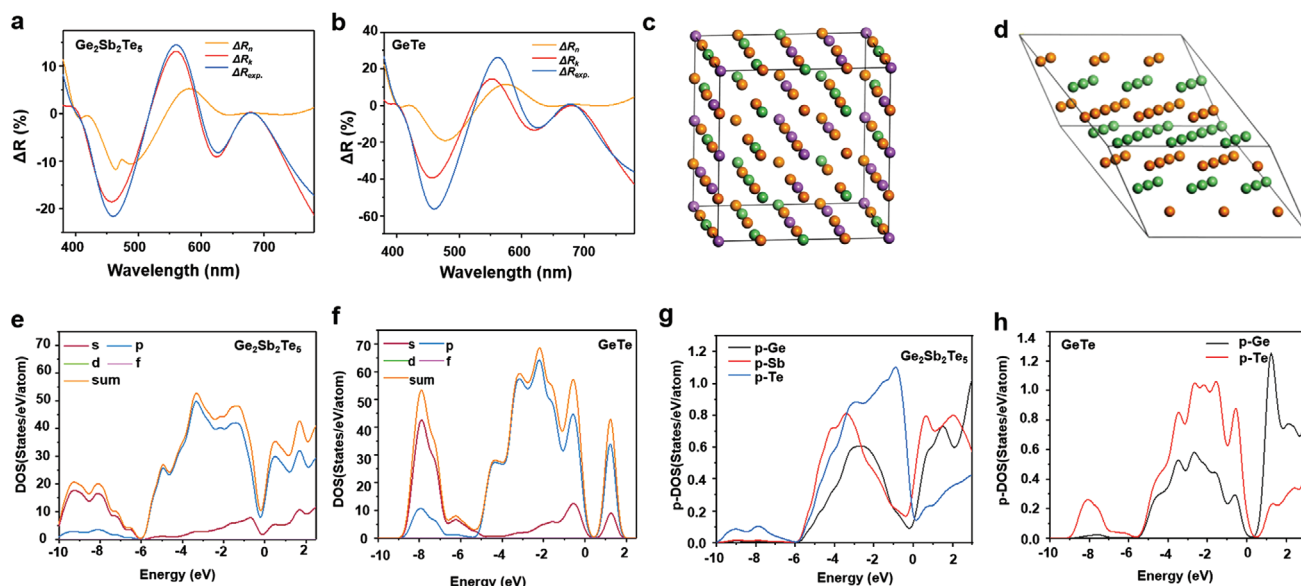


Figure 5. The effect of Δn and Δk on ΔR for a) $\text{Ge}_2\text{Sb}_2\text{Te}_5$ and b) GeTe ; theoretical structure models for c) $\text{c-Ge}_2\text{Sb}_2\text{Te}_5$ and d) c-GeTe , where the yellow balls are Te atoms, the green balls are Ge atoms, and the purple balls are Sb atoms. DOS of e) $\text{c-Ge}_2\text{Sb}_2\text{Te}_5$ and f) c-GeTe ; partial DOS (p-DOS) of g) $\text{c-Ge}_2\text{Sb}_2\text{Te}_5$ and h) c-GeTe .

IPIA $_{\text{Ge}_2\text{Sb}_2\text{Te}_5}$, we calculated the reflectivity difference (ΔR) between IPIA coatings containing amorphous and crystalline PCMs, and the influences of Δn and Δk on ΔR are shown in Figure 5a,b. There is no obvious dependence between ΔR_{exp} and ΔR_n , whereas the peaks at about 460 and 560 nm appear in both ΔR_{exp} and ΔR_k spectra, which have very similar characteristics. This indicates that the ΔR_{exp} (color-changing performance) of the display coating does not originate from Δn but originate from Δk . It can be seen from Figure S5a (Supporting Information) that the extinction coefficients k of c-GeTe is significantly higher than that of $\text{c-Ge}_2\text{Sb}_2\text{Te}_5$. Therefore, the higher color-changing performance of IPIA $_{\text{GeTe}}$ coating is attributed to the higher k value of c-GeTe film.

Why does c-GeTe have a higher k than $\text{c-Ge}_2\text{Sb}_2\text{Te}_5$? According to Equations (3)–(7), the k of film is determined by the amplitude A , broadening term C , central energy E_0 , optical bandgap E_g , and the high-frequency dielectric constant ϵ_{hf} of Lorentz oscillator. Therefore, the difference in k between c-GeTe and $\text{c-Ge}_2\text{Sb}_2\text{Te}_5$ ($\Delta k = k_{\text{c-GeTe}} - k_{\text{c-Ge}_2\text{Sb}_2\text{Te}_5}$) is attributed to the differences in these five parameters (ΔA , ΔC , ΔE_0 , ΔE_g , and $\Delta \epsilon_{\text{hf}}$) between two coatings. We then systematically studied the influence of each parameter (ΔA , ΔC , ΔE_0 , ΔE_g , and $\Delta \epsilon_{\text{hf}}$) on k and obtained the contribution of each parameter to Δk_{exp} (Δk_A , Δk_C , Δk_{E_0} , Δk_{E_g} , $\Delta k_{\epsilon_{\text{hf}}}$) (Figure S5b, Supporting Information). For ease of comparison, the actual difference in k between GeTe and $\text{Ge}_2\text{Sb}_2\text{Te}_5$ (Δk) was also given. Clearly, ΔE_0 , ΔE_g , and $\Delta \epsilon_{\text{hf}}$ have almost no influence on k , while ΔA and ΔC have significant influence on k . This means that the change of degree of order is the main factor leading to change of k . c-GeTe has a larger A and a smaller C than $\text{c-Ge}_2\text{Sb}_2\text{Te}_5$, which means c-GeTe has a higher degree of order than $\text{c-Ge}_2\text{Sb}_2\text{Te}_5$.^[55,56] Therefore, c-GeTe film has a higher k value due to a higher degree of order.

The high degree of order of c-GeTe and the dependence of color changing performance on k can be well understood by the theories of resonant bonding and electron delocalization.^[9,57] We

established two theoretical models of c-GeTe and $\text{c-Ge}_2\text{Sb}_2\text{Te}_5$ by first-principles calculation, in which $\text{c-Ge}_2\text{Sb}_2\text{Te}_5$ has about 20% vacancies (Figure 5c) and c-GeTe has no vacancies (Figure 5d). For c-GeTe and $\text{c-Ge}_2\text{Sb}_2\text{Te}_5$, the density of states (DOS) at the Fermi level is mainly contributed by atomic p-orbital, indicating that strong p–p coupling occurs between atoms in c-GeTe and $\text{c-Ge}_2\text{Sb}_2\text{Te}_5$ (Figure 5e,f). The p–p coupling strengths of c-GeTe and $\text{c-Ge}_2\text{Sb}_2\text{Te}_5$ were obtained by calculating the ratio of the overlapping portion of the partial DOS (Figure 5g,h) of Ge, Sb, and Te atoms to the integrated area of Te, as shown in Figure S5c (Supporting Information). The p–p coupling strength of GeTe ($I_{\text{p-GeTe}} = 50.01$) is higher than that of $\text{Ge}_2\text{Sb}_2\text{Te}_5$ ($I_{\text{p-Ge}_2\text{Sb}_2\text{Te}_5} = 45.13$), which means the lattice distortion of c-GeTe without vacancies is smaller and its degree of structural order is higher. These are more favorable for the overlap hybridization and coupling between p orbitals and the formation of p electrons. As shown in Figure S6 (Supporting Information), the resistance of GeTe film is $0.0609 \, \Omega \, \square^{-1}$, which is $1/59.9$ of that of $\text{Ge}_2\text{Sb}_2\text{Te}_5$; the electron concentration of GeTe is $5.598 \times 10^{21} \, \text{cm}^{-3}$, which is 10 000 times of that of $\text{Ge}_2\text{Sb}_2\text{Te}_5$. Therefore, our calculations are in good agreement with the experimental results, consistently proving that the vacancy-free c-GeTe has a higher degree of structural order than $\text{c-Ge}_2\text{Sb}_2\text{Te}_5$. This enhances the p–p coupling and p-electron delocalization in c-GeTe , further more free electrons are generated and a larger k is obtained.

2.4. Atomic-Level Design of PCMs for Display Coatings with High Color-Changing Performance

The internal vacancy, which is caused by the number of Ge+Sb atoms less than that of Te atom, is ubiquitous in the crystalline phase of phase change materials. In addition to GeTe and $\text{Ge}_2\text{Sb}_2\text{Te}_5$, we also prepared $\text{Ge}_8\text{Sb}_2\text{Te}_{11}$, $\text{Ge}_3\text{Sb}_2\text{Te}_6$, and

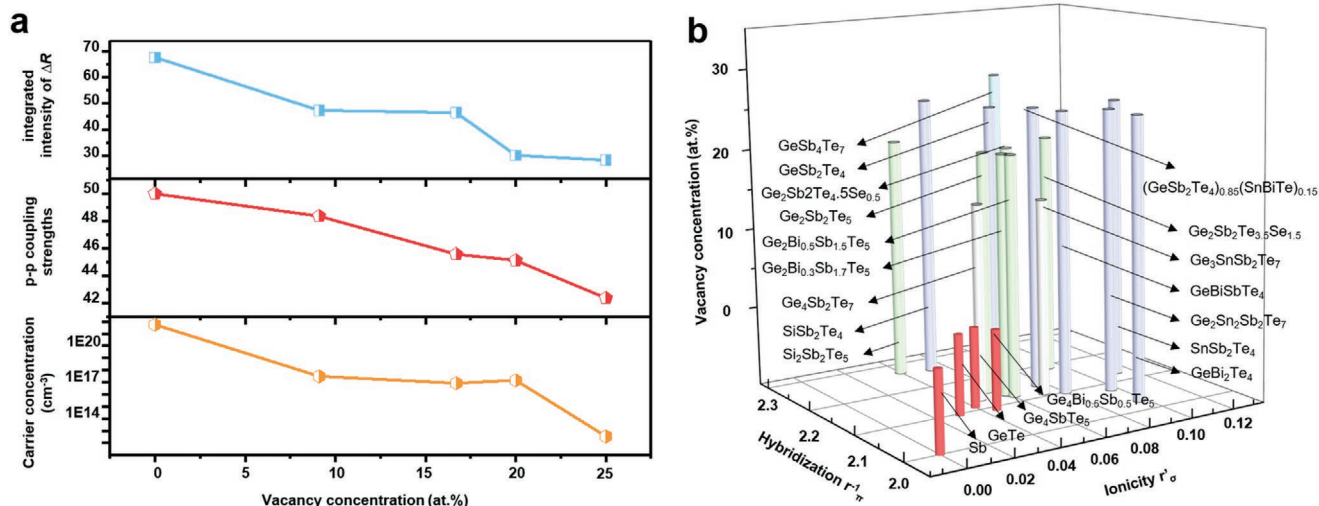


Figure 6. a) The relationship between carrier concentration, p-p coupling strength, integrated intensity of ΔR and vacancy concentration for GeTe , $\text{Ge}_8\text{Sb}_2\text{Te}_{11}$, $\text{Ge}_3\text{Sb}_2\text{Te}_6$, $\text{Ge}_2\text{Sb}_2\text{Te}_5$, and $\text{Ge}_1\text{Sb}_2\text{Te}_4$. b) 3D map of PCMs with different vacancy concentrations, ionicity, and hybridization.

$\text{Ge}_1\text{Sb}_2\text{Te}_4$ on the GeTe - Sb_2Te_3 scale line. These materials can be regarded as the same material, and the relationships among their vacancies and optical constants, thermal conductivity, etc.,^[48,58] have been extensively studied. The vacancy concentration can be calculated by $c_v = (n_{\text{Te}} - n_{\text{Sb}} - n_{\text{Ge}})/n_{\text{Te}}$, where n_{Ge} , n_{Sb} , and n_{Te} represent the atomic numbers of Ge, Sb, and Te, respectively. According to this equation, the vacancy concentrations of GeTe , $\text{Ge}_8\text{Sb}_2\text{Te}_{11}$, $\text{Ge}_3\text{Sb}_2\text{Te}_6$, $\text{Ge}_2\text{Sb}_2\text{Te}_5$, and $\text{Ge}_1\text{Sb}_2\text{Te}_4$ are 0%, 9.1%, 16.6%, 20%, and 25%, respectively.

The influences of vacancy concentration on p-p coupling strength, electron concentration, and color-changing performance is plotted in Figure 6a. Interestingly, as the vacancy concentration increases from 0% to 25% (which means PCM changes from GeTe , $\text{Ge}_8\text{Sb}_2\text{Te}_{11}$, $\text{Ge}_3\text{Sb}_2\text{Te}_6$, $\text{Ge}_2\text{Sb}_2\text{Te}_5$ to $\text{Ge}_1\text{Sb}_2\text{Te}_4$), the p-p coupling strength decreases from 50.01% to 42.37%, the electron concentration decreases from 5.598×10^{21} to $3.518 \times 10^{12} \text{ cm}^{-3}$, and the color-changing performance gradually decreases from 67.66 to 28.17. These results are in good agreement with the previous discussion, which proves that the introduction of vacancy can reduce the p-p coupling strength and the degree of electron delocalization, and thus reduce the color-changing performance of coatings.

On above analysis, we believe that the high color-changing performance of coating comes from its high degree of electron delocalization. Previous studies have shown that high degree electron delocalization is based on low ionicity and low sp^3 -orbital hybridization trends,^[48] which can be calculated by the following equations

$$r_{\pi}^{-1} = \left[\left(\frac{\sum_i n_i (r_{p,i} - r_{s,i})}{\sum_i n_i} \right)_{\text{Anion}} + \left(\frac{\sum_j n_j (r_{p,j} - r_{s,j})}{\sum_j n_j} \right)_{\text{Cations}} \right]^{-1} \quad (1)$$

$$r'_{\sigma} = \left(\frac{\sum_i n_i (r_{p,i} - r_{s,i})}{\sum_i n_i} \right)_{\text{Anion}} - \left(\frac{\sum_j n_j r_{p,j}}{\sum_j n_j} \right)_{\text{Cation}} \quad (2)$$

According to the above two equations, low ionicity and a limited degree of hybridization are based on small difference between p-orbital radii and large difference between s- and p-orbital radii. According to these two principles, researchers have found that high optical contrast PCMs are mainly Te-based binary or ternary materials, such as GeTe , Sb_2Te_3 , $\text{Ge}_2\text{Sb}_2\text{Te}_5$, $\text{Ge}_1\text{Sb}_2\text{Te}_4$, and so on. Notably, our research shows that high p-p coupling strength is another important condition for generating high degree electron delocalization. Therefore, we propose the following three principles for designing PCM-based display coatings with high color-changing performance: 1) low ionicity of atoms; 2) a limited degree of hybridization; 3) high p-p coupling strength. As shown in Figure 6a, there is a strong inverse relationship between coupling strength and vacancy concentration. In order to simplify the calculation, the vacancy concentration was used to approximate the p-p coupling strength. Figure 6b shows the ionicity, sp^3 -orbital hybridization, and vacancy concentration of Te-based binary or ternary materials. It can be seen that Sb, GeTe , $\text{Ge}_4\text{Sb}_2\text{Te}_7$, $\text{Ge}_4\text{Bi}_{0.5}\text{Sb}_{0.5}\text{Te}_5$ meet all the principles at the same time. They are thus ideal candidates for display coatings with high color-changing performance and worthy of further study.

3. Conclusions

This study successfully revealed the color-changing mechanism of ITO/PCM/ITO/Ag four-layer coatings and proposed, for the first time, the structural design principles of PCMs for display coatings with high color-changing performance. The experiments, theoretical calculations, spectral fitting, and optical simulation agree well with each other, consistently proving the following conclusions:

- 1) The color-changing performance of PCM-based IPIA display coatings depends strongly on the extinction coefficient contrast instead of refractive index contrast between the amorphous and crystalline states of PCM. The underlying

color-changing mechanism is that phase change leads to a highly ordered structure and electron delocalization, which induces the difference in extinction coefficient between crystalline and amorphous states of PCM. This finally leads to the changes of the reflectivity and color of the IPIA four-layer display coating.

- 2) The color-changing performance of PCM-based IPIA display coatings follows the order: GeTe > Ge₈Sb₂Te₁₁ > Ge₃Sb₂Te₆ > Ge₂Sb₂Te₅ > Ge₁Sb₂Te₄. This is attributed to the increase of vacancy concentration, which significantly reduces the degree of structural order and p-p coupling strength and further reduces electron delocalization and extinction coefficient contrast. The vacancy-free GeTe-based IPIA display coating was found to have the optimal color-changing performance, and its p-p coupling strength, color contrast, and number of hues are 11.1%, 124.8%, and 50.0% higher than those of vacancy-containing Ge₂Sb₂Te₅-based IPIA coatings, respectively.
- 3) According to our new insights into the p-p coupling strength and previous reports by Wuttig et al., we believe that the ideal PCMs used for display coatings should have the following three features of electronic structure: a) low ionicity; b) limited degree of hybridization; c) high p-p coupling strength. Based on the three structural design principles above, it is predicted that Sb, Ge₄Sb₇Te₅, Ge₄Bi_{0.5}Sb_{0.5}Te₅, and other vacancy-free PCMs also have high color-changing performance in addition to GeTe, and these PCMs are worthy of in-depth study and experimental verification.

4. Experimental Section

All the films were deposited simultaneously onto single crystal Si (001) and optical glass substrates by RF magnetron sputtering. The deposition process was carried out under a pressure of 0.416 Pa and a pure Ar atmosphere with a flow rate of 56 sccm. The power applied to the Ag target and the ITO target were 100 and 80 W, respectively. The power applied to GeTe, Ge₈Sb₂Te₁₁, Ge₃Sb₂Te₆, Ge₂Sb₂Te₅ to Ge₁Sb₂Te₄ target were both 10 W for multilayer films and both 60 W for single layer films (with thickness of about 200 nm). During deposition, no additional bias was applied to the substrates. The as-deposited samples were annealed in an Ar atmosphere using a tube furnace for 30 min at a heating rate of 3 °C min⁻¹.

A grazing incidence X-ray diffraction measurement (D8tools, Cu K α , Bruker, Karlsruhe, Germany), SAED and high-resolution transmission electron microscopy (JEM-2100F, JEOL, Tokyo, Japan) were performed to characterize the structures of films. The thickness of each film was measured using a Dektak 3 surface profiler. The reflectance spectra of films at room temperature were measured using a UV-vis-NIR spectrometer (Lambda 950, PerkinElmer, US). The measurement step and wavelength range were set to 2 and 400–760 nm, respectively. The chemical composition of the sample was analyzed by energy dispersive spectroscopy equipped in the SEM (SU8010, HITACHI, Japan). The results are Ge₁Sb₂Te₄ (1:2.4:4.06), Ge₂Sb₂Te₅ (2:2.19:4.76), Ge₃Sb₂Te₆ (3:2.16:5.38), Ge₈Sb₂Te₁₁ (8:2.26:10.74), and GeTe (1:1), which is basically the same as the composition of targets.

The reflectance spectra were fitted using the Tauc–Lorentz model^[59] based on the Tauc joint density of states and the Lorentz oscillator. This model has been widely used to fit and analyze the reflectance spectra of PCMs. The related equations are given as follows

$$R = \frac{(n-1)^2 + k^2}{(n+1)^2 + k^2} \quad (3)$$

$$\varepsilon_1 = n^2 - k^2 \quad (4)$$

$$\varepsilon_2 = 2nk \quad (5)$$

$$\varepsilon_2 = \begin{cases} \frac{AE_n C (E - E_g)^2}{(E^2 - E_0^2)^2 + C^2 E^2} \cdot \frac{1}{E} & E > E_g \\ 0 & E \leq E_g \end{cases} \quad (6)$$

$$\varepsilon_1 = \varepsilon_{\text{hf}} + \frac{2}{\pi} P \int_{E_g}^{\infty} \frac{\xi \varepsilon_2}{\xi^2 - E^2} d\xi \quad (7)$$

where R is the reflectance of film; n , k , ε_1 , and ε_2 are the refractive index, extinction coefficient, real part, and imaginary part of the dielectric function, respectively; A , E_0 , C , and E_g are the amplitude, peak transition energy, broadening term, and optical bandgap, respectively; ε_{hf} is the high frequency dielectric constant; E is the incident photon energy; P is the Cauchy principal part of the integral.

The DOS and p-DOS spectra of Ge₂Sb₂Te₅ and GeTe were calculated by the CASTEP model based on density functional theory.^[60] There was a total of 58 atoms (including 13 Ge atoms, 13 Sb atoms, and 32 Te atoms) and 6 vacancies in the cubic Ge₂Sb₂Te₅. The lattice constant was set to 0.601 nm. The space group of crystalline rhombohedral GeTe was 160 $R3m$, and the lattice parameters were set to $a = b = 0.4231$ nm, $c = 1.0890$ nm, $\alpha = \beta = 90^\circ$, and $\gamma = 120^\circ$. The cutoff energy and the K point were set to 205 eV and $2 \times 2 \times 2$, respectively.

Supporting Information

Supporting Information is available from the Wiley Online Library or from the author.

Acknowledgements

S.T. and Q.L. contributed equally to this work. The authors gratefully acknowledge the financial support from National Natural Science Foundation of China (Grant Nos. 51572104, 51672101, and 51602122), National Key R&D Program of China (No. 2016YFA0200400), National Major Project for Research on Scientific Instruments of China (No. 2012YQ24026404), Fundamental Research Funds for the Central Universities (JLU), Program for JLU Science and Technology Innovative Research Team (JLUJSTRT, 2017TD-09).

Conflict of Interest

The authors declare no conflict of interest.

Keywords

color-changing performance, nonvolatile coatings, phase change materials, reflective displays, structural design

Received: January 10, 2020
Published online: March 12, 2020

- [1] T. Cao, X. Zhang, W. Dong, L. Lu, X. Zhou, X. Zhuang, J. Deng, X. Cheng, G. Li, R. E. Simpson, *Adv. Opt. Mater.* **2018**, 6, 1800169.
- [2] F. Ding, Y. Yang, S. I. Bozhevolnyi, *Adv. Opt. Mater.* **2019**, 7, 1801709.

- [3] R. E. Simpson, P. Fons, A. V. Kolobov, T. Fukaya, M. Krbal, T. Yagi, J. Tominaga, *Nat. Nanotechnol.* **2011**, 6, 501.
- [4] C. Choi, S. Y. Lee, S. E. Mun, G. Y. Lee, J. Sung, H. Yun, J. H. Yang, H. O. Kim, C. Y. Hwang, B. Lee, *Adv. Opt. Mater.* **2019**, 7, 1900171.
- [5] D. Loke, T. H. Lee, W. J. Wang, L. P. Shi, R. Zhao, Y. C. Yeo, T. C. Chong, S. R. Elliott, *Science* **2012**, 336, 1566.
- [6] K. V. Sreekanth, Q. Ouyang, S. Sreejith, S. Zeng, W. Lishu, E. Ilker, W. Dong, M. ElKabbash, Y. Ting, C. T. Lim, M. Hinczewski, G. Strangi, K. T. Yong, R. E. Simpson, R. Singh, *Adv. Opt. Mater.* **2019**, 7, 1900081.
- [7] M. Wuttig, M. Salinga, *Nat. Mater.* **2012**, 11, 270.
- [8] T. Cao, Y. Cao, L. Fang, *Nanoscale* **2019**, 11, 15828.
- [9] K. Shportko, S. Kremers, M. Woda, D. Lencer, J. Robertson, M. Wuttig, *Nat. Mater.* **2008**, 7, 653.
- [10] T. H. Lee, D. Loke, S. R. Elliott, *Adv. Mater.* **2015**, 27, 5477.
- [11] L. Waldecker, T. A. Miller, M. Rude, R. Bertoni, J. Osmond, V. Pruneri, R. E. Simpson, R. Ernstorfer, S. Wall, *Nat. Mater.* **2015**, 14, 991.
- [12] J. M. Skelton, A. R. Pallipurath, T. H. Lee, S. R. Elliott, *Adv. Funct. Mater.* **2014**, 24, 7291.
- [13] G. M. Zewdie, Y. Zhou, L. Sun, F. Rao, V. L. Deringer, R. Mazzarello, W. Zhang, *Chem. Mater.* **2019**, 31, 4008.
- [14] T. A. Miller, M. Rude, V. Pruneri, S. Wall, *Phys. Rev. B* **2016**, 94, 024301.
- [15] M. Salinga, B. Kersting, I. Ronneberger, V. P. Jonnalagadda, X. T. Vu, M. Le Gallo, I. Giannopoulos, O. Cojocaru-Miredin, R. Mazzarello, A. Sebastian, *Nat. Mater.* **2018**, 17, 681.
- [16] F. Rao, Z. T. Song, Y. Cheng, X. S. Liu, M. J. Xia, W. Li, K. Y. Ding, X. F. Feng, M. Zhu, S. L. Feng, *Nat. Commun.* **2015**, 6, 10040.
- [17] X. Zhou, L. Wu, Z. Song, Y. Cheng, F. Rao, K. Ren, S. Song, B. Liu, S. Feng, *Acta Mater.* **2013**, 61, 7324.
- [18] X. Zhou, L. Wu, Z. Song, F. Rao, M. Zhu, C. Peng, D. Yao, S. Song, B. Liu, S. Feng, *Appl. Phys. Lett.* **2012**, 101, 142104.
- [19] X. Zhou, M. Xia, F. Rao, L. Wu, X. Li, Z. Song, S. Feng, H. Sun, *ACS Appl. Mater. Interfaces* **2014**, 6, 14207.
- [20] D. K. Loke, J. M. Skelton, T. H. Lee, R. Zhao, T. C. Chong, S. R. Elliott, *ACS Appl. Mater. Interfaces* **2018**, 10, 41855.
- [21] D. K. Loke, G. J. Clausen, J. F. Ohmura, T.-C. Chong, A. M. Belcher, *ACS Appl. Nano Mater.* **2018**, 1, 6556.
- [22] M. Salinga, E. Carria, A. Kaldebach, M. Bornhoff, J. Benke, J. Mayer, M. Wuttig, *Nat. Commun.* **2013**, 4, 2371.
- [23] T. H. Lee, D. Loke, K. J. Huang, W. J. Wang, S. R. Elliott, *Adv. Mater.* **2014**, 26, 7493.
- [24] B. Hauer, T. Saltzmann, U. Simon, T. Taubner, *Nano Lett.* **2015**, 15, 2787.
- [25] W. Dong, Y. Qiu, X. Zhou, A. Banas, K. Banas, M. B. H. Breese, T. Cao, R. E. Simpson, *Adv. Opt. Mater.* **2018**, 6, 1701346.
- [26] C. Rios, P. Hosseini, R. A. Taylor, H. Bhaskaran, *Adv. Mater.* **2016**, 28, 4720.
- [27] P. Hosseini, C. D. Wright, H. Bhaskaran, *Nature* **2014**, 511, 206.
- [28] K. K. Du, Q. Li, Y. B. Lyu, J. C. Ding, Y. Lu, Z. Y. Cheng, M. Qiu, *Light: Sci. Appl.* **2017**, 6, e16194.
- [29] P. Pitchappa, A. Kumar, S. Prakash, H. Jani, T. Venkatesan, R. Singh, *Adv. Mater.* **2019**, 31, e1808157.
- [30] T. Cao, K. Liu, L. Lu, H. C. Chui, R. E. Simpson, *ACS Appl. Mater. Interfaces* **2019**, 11, 5176.
- [31] V. K. Mkhitarian, D. S. Ghosh, M. Rudé, J. Canet-Ferrer, R. A. Maniyara, K. K. Gopalan, V. Pruneri, *Adv. Opt. Mater.* **2017**, 5, 1600452.
- [32] Y. Qu, Q. Li, L. Cai, M. Pan, P. Ghosh, K. Du, M. Qiu, *Light: Sci. Appl.* **2018**, 7, 26.
- [33] A. Lotnyk, U. Ross, T. Dankwort, I. Hilmi, L. Kienle, B. Rauschenbach, *Acta Mater.* **2017**, 141, 92.
- [34] X. Yin, T. Steinle, L. Huang, T. Taubner, M. Wuttig, T. Zentgraf, H. Giessen, *Light: Sci. Appl.* **2017**, 6, e17016.
- [35] C. D. Wright, H. Bhaskaran, W. H. P. Pernice, *MRS Bull.* **2019**, 44, 721.
- [36] M. Wuttig, H. Bhaskaran, T. Taubner, *Nat. Photonics* **2017**, 11, 465.
- [37] F. F. Schlich, P. Zalden, A. M. Lindenberg, R. Spolenak, *ACS Photonics* **2015**, 2, 178.
- [38] C. Y. Hwang, G. H. Kim, J. H. Yang, C. S. Hwang, S. M. Cho, W. J. Lee, J. E. Pi, J. H. Choi, K. Choi, H. O. Kim, S. Y. Lee, Y. H. Kim, *Nanoscale* **2018**, 10, 21648.
- [39] S. G. C. Carrillo, L. Trimby, Y. Y. Au, V. K. Nagareddy, G. Rodriguez-Hernandez, P. Hosseini, C. Rios, H. Bhaskaran, C. D. Wright, *Adv. Opt. Mater.* **2019**, 7, 1801782.
- [40] C. Talagrand, G. Triggs, L. Bandhu, S. Garcia-Castillo, B. Broughton, H. Bhaskaran, P. Hosseini, *J. Soc. Inf. Disp.* **2018**, 26, 619.
- [41] Z. Ni, S. Mou, T. Zhou, Z. Cheng, *Appl. Opt.* **2018**, 57, 3385.
- [42] Y. Lyu, S. Mou, Z. Ni, Y. Bai, Y. Sun, Z. Cheng, *Opt. Express* **2017**, 25, 1405.
- [43] F. Liu, H. Shi, X. Zhu, P. Dai, Z. Lin, Y. Long, Z. Xie, Y. Zhou, H. Duan, *Appl. Opt.* **2018**, 57, 9040.
- [44] S. Yoo, T. Gwon, T. Eom, S. Kim, C. S. Hwang, *ACS Photonics* **2016**, 3, 1265.
- [45] H. K. Ji, H. Tong, H. Qian, Y. J. Hui, N. Liu, P. Yan, X. S. Miao, *Sci. Rep.* **2016**, 6, 39206.
- [46] M. Jafari, L. J. Guo, M. Rais-Zadeh, *Adv. Opt. Mater.* **2019**, 7, 1801214.
- [47] P. A. Vermeulen, D. T. Yimam, M. A. Loi, B. J. Kooi, *J. Appl. Phys.* **2019**, 125, 193105.
- [48] D. Lencer, M. Salinga, B. Grabowski, T. Hickel, J. Neugebauer, M. Wuttig, *Nat. Mater.* **2008**, 7, 972.
- [49] J.-W. Park, S. H. Eom, H. Lee, J. L. F. Da Silva, Y.-S. Kang, T.-Y. Lee, Y. H. Khang, *Phys. Rev. B* **2009**, 80, 115209.
- [50] C. Peng, F. Rao, L. Wu, Z. Song, Y. Gu, D. Zhou, H. Song, P. Yang, J. Chu, *Acta Mater.* **2014**, 74, 49.
- [51] Y. Wang, T. Guo, G. Liu, T. Li, S. Lv, S. Song, Y. Cheng, W. Song, K. Ren, Z. Song, *ACS Appl. Mater. Interfaces* **2019**, 11, 10848.
- [52] T. Ohta, M. Uchida, K. Yoshioka, K. Inoue, T. Aiyama, S. Furukawa, K. Kotera, S. Nakamura, *Proc. SPIE* **1989**, 1078, 27.
- [53] T. Ohta, K. Inoue, M. Uchida, K. Yoshioka, T. Akiyama, S. Furukawa, K. Nagata, S. Nakamura, *Jpn. J. Appl. Phys.* **1989**, 28, 123.
- [54] T. C. Chong, L. P. Shi, W. Qiang, P. K. Tan, X. S. Miao, X. Hu, *J. Appl. Phys.* **2002**, 91, 3981.
- [55] P. Němec, J. Přikryl, V. Nazabal, M. Frumar, *J. Appl. Phys.* **2011**, 109, 073520.
- [56] S. Guo, L. Xu, J. Zhang, Z. Hu, T. Li, L. Wu, Z. Song, J. Chu, *Sci. Rep.* **2016**, 6, 33639.
- [57] M. Wuttig, V. L. Deringer, X. Gonze, C. Bichara, J. Y. Raty, *Adv. Mater.* **2018**, 30, e1803777.
- [58] K. S. Siegfert, F. R. Lange, E. R. Sittner, H. Volker, C. Schlockermann, T. Siegrist, M. Wuttig, *Rep. Prog. Phys.* **2015**, 78, 013001.
- [59] S. Guo, M. J. Li, Q. Q. Li, Z. G. Hu, T. Li, L. C. Wu, Z. T. Song, J. H. Chu, *Appl. Phys. Lett.* **2017**, 110, 161906.
- [60] C. Li, C. Hu, J. Wang, X. Yu, Z. Yang, J. Liu, Y. Li, C. Bi, X. Zhou, W. Zheng, *J. Mater. Chem. C* **2018**, 6, 3387.